Broadband wavelength conversion in a silicon vertical-dual-slot waveguide

Guo, Kai; Lin, Li; Christensen, Jesper Bjerge; Christensen, Erik Nicolai; Shi, Xiaodong; Ding, Yunhong; Rottwitt, Karsten; Ou, Haiyan

Published in:
Optics Express

Link to article, DOI:
10.1364/OE.25.032964

Publication date:
2017

Document Version
Publisher's PDF, also known as Version of record

Research Article | Vol. 25, No. 26 | 25 Dec 2017 | OPTICS EXPRESS 32964
Optics EXPRESS

Broadband wavelength conversion in a silicon vertical-dual-slot waveguide

KAI GUO,[1,2] LI LIN,[2] JESPER B. CHRISTENSEN,[2] ERIK N. CHRISTENSEN,[2] XIAODONG SHI,[2] YUNHONG DING,[2] KARSTEN ROTTWITT[2] AND HAIYAN OU[2,*]

[1]*College of Optoelectronic Science and Engineering, National University of Defense Technology, Changsha 410073, Hunan, China*
[2]*Department of Photonics Engineering, Technical University of Denmark, Kgs. Lyngby 2800, Denmark*
[*] *haou@fotonik.dtu.dk*

Abstract: We propose a silicon waveguide structure employing silica-filled vertical-dual slots for broadband wavelength conversion, which can be fabricated using simple silicon-on-insulator technology. We demonstrate group-velocity dispersion tailoring by varying the width of the core, the slots and the side strips, and put forward a method to achieve spectrally-flattened near-zero anomalous group-velocity dispersion at telecom wavelengths. A proposed structure provides a group-velocity dispersion parameter β_2 of -60 ps^2/km with an effective mode area A_{eff} of 0.075 μm^2 at 1550 nm. This structure is predicted to significantly broaden the bandwidth of wavelength conversion via four-wave mixing, which is validated with experimentally measured 3 dB bandwidth of 76 nm.

OCIS codes: (130.4310) Nonlinear; (190.4360) Nonlinear optics, devices; (190.4380) Nonlinear optics, four-wave mixing

References and links

1. C. Koos, P. Vorreau, T. Vallaitis, P. Dumon, W.Bogaerts, R. Baets, B. Esembeson, I. Biaggio, T. Michinobu, F. Diederich, W. Freude, and J. Leuthold "All-optical high-speed signal processing with silicon–organic hybrid slot waveguides," Nature **3**(4), 216–219 (2009).
2. J. E. Sharping, K. F. Lee, M. A. Foster, A. C. Turner, B. S. Schmidt, M. Lipson, L. G. Alexander, and P. Kumar, "Generation of correlated photons in nanoscale silicon waveguides," Opt. Express **14**(25), 12388–12393 (2006).
3. K. Guo, E. N. Christensen, J. B. Christensen, J. G. Koefoed, D. Bacco, Y. Ding, H. Ou and K. Rottwitt, "High coincidence-to-accidental ratio continuous-wave photon-pair generation in a grating-coupled silicon strip waveguide," Appl. Phys. Express **10**(6), 062801 (2017).
4. Y. Ding, J. Xu, H. Ou, and C. Peucheret, "Mode-selective wavelength conversion based on four-wave mixing in a multimode silicon waveguide," Opt. Express **22**(1), 127–135 (2014).
5. M. Pu, H. Hu, C. Peucheret, H. Ji, M. Galili, L. K. Oxenløwe, and K. Yvind, "Polarization insensitive wavelength conversion in a dispersion-engineered silicon waveguide," Opt. Express **20**(15), 16374–16380 (2012).
6. H. Hu, J. D. Andersen, A. Rasmussen, B. M. Sørensen, K. Dalgaard, M. Galili, and L. K. Oxenløwe, "Forward error correction supported 150 Gbit/s error-free wavelength conversion based on cross phase modulation in silicon," Opt. Express **21**(3), 3152–3160 (2013).
7. J. Hansryd, P. A. Andrekson, M. Westlund, J. Li, and P. O. Hedekvist, "Fiber-based optical parametric amplifiers and their applications," IEEE J. Sel. Top. Quantum Electron. **8**(3), 506–520 (2002).
8. L. Zhang, Y. Yue, R. G. Beausoleil, and A. E. Willner, "Flattened dispersion in silicon slot waveguides," Opt. Express **18**(19), 20529–20534 (2010).
9. P. Muellner, and R. Hainberger, "Structural optimization of silicon-on-insulator slot waveguides," IEEE Photonics Technol. Lett. **18**(24), 2557–2559 (2006).
10. P. Sanchis, J. Blasco, A. Martínez, J. and Martí, "Design of silicon-based slot waveguide configurations for optimum nonlinear performance," J. Lightwave Technol. **25**(5), 1298–1305 (2007).
11. R. Sun, P. Dong, N. Feng, C. Y. Hong, J. Michel, M. Lipson, and L. Kimerling, "Horizontal single and multiple slot waveguides: optical transmission at λ = 1550 nm," Opt. Express **15**(26), 17967–17972 (2007).
12. Y. C. Jun, R. M. Briggs, H. A. Atwater, and M. L. Brongersma, "Broadband enhancement of light emission in silicon slot waveguides," Opt. Express **17**(9), 7479–7490 (2009).

#307962 https://doi.org/10.1364/OE.25.032964
Journal © 2017 Received 26 Sep 2017; revised 27 Nov 2017; accepted 7 Dec 2017; published 19 Dec 2017

Optics EXPRESS

13. P. Muellner, M. Wellenzohn, and R. Hainberger, "Nonlinearity of optimized silicon photonic slot waveguides," Opt. Express **17** (11), 9282–9287 (2009).
14. K. Preston and M. Lipson, "Slot waveguides with polycrystalline silicon for electrical injection," Opt. Express **17**(3), 1527–1534 (2009).
15. M. Galli, D. Gerace, A. Politi, M. Liscidini, M. Patrini, L.C. Andreani, and F. Priolo, "Direct evidence of light confinement and emission enhancement in active silicon-on-insulator slot waveguides," Appl. Phys. Lett. **89**(24), 241114 (2006).
16. A. Martínez, J. Blasco, P. Sanchis, J. V. Galán, J. E. Jordana, and R. Guider, "Ultrafast all-optical switching in a silicon-nanocrystal-based silicon slot waveguide at telecom wavelengths," Nano Lett. **10**(4), 1506–1511 (2010).
17. L. Zhang, Q. Lin, Y.Yue, Y. Yan, R. G. Beausoleil, and A. E. Willner, "Silicon waveguide with four zero-dispersion wavelengths and its application in on-chip octave-spanning supercontinuum generation," Opt. Express **20**(2), 1685–1690 (2012).
18. C. Bao, Y. Yan, L. Zhang, Y. Yue, N. Ahmed, A. M. Agarwal, and A. E. Willner, "Increased bandwidth with flattened and low dispersion in a horizontal double-slot silicon waveguide," J. Opt. Soc. Am. **32**(1), 26–30 (2015).
19. C. A.Barrios and M. Lipson, "Electrically driven silicon resonant light emitting device based on slot-waveguide," Opt. Express **13**(25), 10092–10101 (2005).
20. P. A. Anderson, B. S. Schmidt, and M. Lipson, "High confinement in silicon slot waveguides with sharp bends," Opt. Express **14**(20), 9197–9202 (2006).
21. F. Dellólio and V. M. Passaro, "Optical sensing by optimized silicon slot waveguides," Opt. Express **15**(8), 4977–4993 (2007).
22. C. Koos, P. Vorreau, T. Vallaitis, P. Dumon, W. Bogaerts, R. Baets, and W. Freude, "All-optical high-speed signal processing with silicon-organic hybrid slot waveguides," Nature **3**(4), 216–219 (2009).
23. A. H. Yang, S. D. Moore, B. S. Schmidt, M. Klug, M. Lipson, and D. Erickson, "Optical manipulation of nanoparticles and biomolecules in sub-wavelength slot waveguides," Nature **457**(7225), 71–75 (2009).
24. R. Ding, T. Baehr-Jones, W. J. Kim, B. Boyko, R. Bojko, A. Spott, and M. Hochberg, "Low-loss asymmetric strip-loaded slot waveguides in silicon-on-insulator," Appl. Phys. Lett. **98**(23), 233303 (2011).
25. M. Gould, T. Baehr-Jones, R. Ding, S. Huang, J. Luo, A. K. Y. Jen, and M. Hochberg, "Silicon-polymer hybrid slot waveguide ring-resonator modulator," Opt. Express **19**(5), 3952–3961 (2011).
26. P. W. Nolte, C. Bohley, and J. Schilling, "Tuning of zero group velocity dispersion in infiltrated vertical silicon slot waveguides," Opt. Express **21**(2), 1741–1750 (2013).
27. W. Zhang, S. Serna, X. Le Roux, C. Alonso-Ramos, L. Vivien, and E. Cassan, "Analysis of silicon-on-insulator slot waveguide ring resonators targeting high Q-factors," Opt. Lett. **40**(23), 5566–5569 (2015).
28. M. Zhu, H. Liu, X. Li, N. Huang, Q. Sun, Wen , and Z. Wang, "Ultrabroadband flat dispersion tailoring of dual-slot silicon waveguides," Opt. Express **20**(14), 15899–15907 (2012).
29. R. F. W. Pease, "Electron beam lithography," Contemporary Phys. **22**(3), 265–290 (1981).
30. J. K. Bhardwaj, and H. Ashraf, "Advanced silicon etching using high-density plasmas," in *Micromachining and Microfabrication* (ISOP 1995), pp. 224–233.
31. A. Säynätjoki, T. Alasaarela, A.Khanna, L. Karvonen, P. Stenberg, M. Kuittinen, and S. Honkanen, "Angled sidewalls in silicon slot waveguides: conformal filling and mode properties," Opt. Express **17** (23), 21066–21076 (2009).
32. E. Jordana, J.M. Fedeli, P. Lyan, J.P. Colonna, P.E. Gautier, N. Daldosso, L. Pavesi, Y. Lebour, P. Pellegrino, B. Garrido, J. Blasco, T. Cuesta-Soto, P. Sanchis, "Deep-UV Lithography Fabrication of SlotWaveguides and Sandwiched Waveguides for Nonlinear Applications," in *2007 4th IEEE International Conference on Group IV Photonics* (IEEE, 2007), paper ThC3.
33. V. R.Almeida, Q. Xu, C. A. Barrios, and M. Lipson, "Guiding and confining light in void nanostructure," Opt. Lett. **29**(11), 1209–1211 (2004).
34. A. B. Fallahkhair, K. S. Li, and T.E. Murphy, "Vector finite difference modesolver for anisotropic dielectric waveguides," J. Lightwave Technol. **26**(11), 1423-1431 (2008).
35. T. A. Birks, J. C. Knight, and P. St. J. Russell, "Endlessly single-mode photonic crystal fiber," Opt. Lett. **22**(13), 961–963 (1997)
36. Y. Ding, H. Ou, and C. Peucheret, "Ultrahigh-efficiency apodized grating coupler using fully etched photonic crystals", Opt. Lett. **38**(15), 2732–2734 (2013).
37. K. Guo, S. M. M. Friis, J. B. Christensen, E. N. Christensen, X. Shi, Y. Ding, H. Ou, and K. Rottwitt, "Full-vectorial propagation model and modified effective mode area of four-wave mixing in straight waveguides," Opt. Lett. **42**(18), 3670–3673 (2017).
38. L. Karvonen, A. Saynatjoki, Y. Chen, X. Tu, T. Y. Liow, J. Hiltunen, M. Hiltunen, G. Lo, and S. Honkanen, " Low-loss multiple-slot waveguides fabricated by optical lithography and atomic layer deposition," IEEE Photonics Technol. Lett. **24**(22), 2074–2076 (2012).

1. Introduction

Four-wave mixing (FWM) in silicon waveguides makes possible a number of key features within classical optical communication systems, such as all-optical signal processing [1], and

Optics EXPRESS

within quantum communication systems, such as photon-pair generation [2, 3]. The most studied technology is wavelength conversion [4–6] via degenerate FWM, which requires highly nonlinear silicon waveguides with engineered group-velocity dispersion (GVD). More specifically, efficient FWM takes place when phase matching is satisfied, which requires an anomalous GVD to cancel the Kerr-induced nonlinear phase shift [7]. Such anomalous GVD is characterized by $\beta_2(\omega_p)<0$, where β_2 is the second-order derivative of the propagation constant and ω_p is the pump frequency. Moreover, in wavelength converters, special effort is made to ensure a broad bandwidth. Therefore, a near-zero GVD at the pump wavelength is desired ($|\beta_2(\omega_p)| \approx 0$) so that phase matching is satisfied at a large pump-signal detuning, where the region in between benefits from effective parametric gain. Additionally, spectrally-flattened GVD also attracts research interest in applications such as supercontinuum generation [8].

The key resource for GVD tailoring is to design the cross-sectional dimension of the waveguide. Previous research has mainly focused on the geometry of the silicon core [4], but this provides only few degrees of freedom, hence it remains a challenge to achieve spectrally-flattened near-zero anomalous GVD. Recently, sandwich structures [8–18] and slot structures [17–28] with flexible geometrical dimension have been developed. The basic concept of these structures is to introduce slots between silicon strips, and use other materials to fill the slots. Based on the mature standard silicon-on-insulator (SOI) technology, the vertical-slot structure is more feasible than the horizotal-sandwich structure because the silicon strips and the slots can be fabricated simultaneously [29, 30]. Meanwhile, the cladding and the slots can be designed to have the same material. Therefore, the fabrication procedure of GVD-engineered slot structure is more convenient than that of the sandwich structure, in which multilayers require extra accurate deposition steps. Note that partial filling of the slots may take place due to the nonuniform deposition, which however can be mitigated by using the suitable deposition procedures [31, 32].

In this paper, we propose a new structure of silicon waveguides that employs silica-filled vertical-dual slots. In our structure, the field is mainly confined in the silicon core, rather than in the slot as the single-slot structures [19–27, 33]. Although an ultra-small effective mode area A_{eff} can be achieved when the optical field is mainly confined in the single slot, such a small A_{eff} does not always enable an ultra-high nonlinear coefficient γ, given by $\gamma = \omega n_2/cA_{\text{eff}}$. Therefore, by using a slot material with smaller intensity-dependent nonlinear refractive index n_2 than silicon, such as silica, may result in a lower nonlinear coefficient. Moreover, the refractive index contrast along the horizontal direction between the center core and the equivalent cladding, silicon side strips included for the proposed structure, is smaller than that for the corresponding silica-cladded strip structure. The reduction in refractive index difference enables a larger degree of control over the anomalous waveguide dispersion, which can be tailored to carefully compensate the normal material dispersion of silicon. This stands in contrast to the case of the strip structure, in which the waveguide dispersion typically over-compensates the silicon dispersion. Here, we demonstrate GVD tailoring by varying the width of the core (W_c), the slots (S) and the side strips (W_s), and put forward a method to obtain spectrally-flattened near-zero anomalous GVD in the telecom wavelength range, including S-, C- and L-band (1460 nm-1625 nm), by shifting the zero-dispersion wavelengths. We take the silica filling ratio of the slots into account, and discuss its impact on GVD. Moreover, by using standard SOI technology, we fabricate a sample and demonstrate a wavelength conversion experiment, which to our best knowledge is the first explicit proof of the proposed structure.

2. Numerical GVD tailoring

In our proposed structure, the slots and the side strips are located symmetrically on both sides of the center core, as shown in Fig. 1. We initially assume that the slots are fully filled, and therefore all regions except the center core and the side strips, are assumed to have the refractive index of silica. The height of the center core and the side strips is 250 nm, determined by the silicon layer

Optics EXPRESS

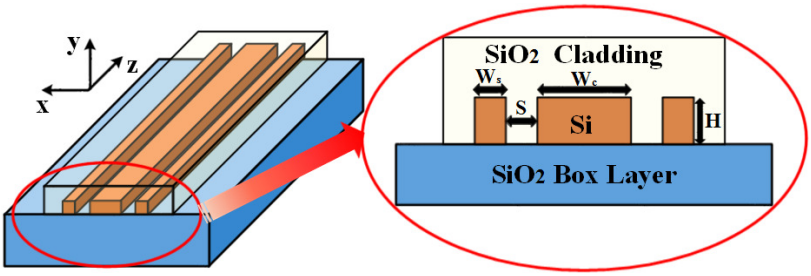

Fig. 1. The vertical-dual-slot structure. H: the height, W_c: the width of the center core, S: the width of the slots, W_s: the width of the side strips.

thickness of the SOI wafer. We focus on the fundamental transverse electric (TE_{01}) mode, and use a finite difference mode solver [34] to simulate the mode profile. As the proposed structure is symmetric, we use the labels W_c-S-W_s (width of core-slot-side strip, in units of nanometers) to represent the different dimensions.

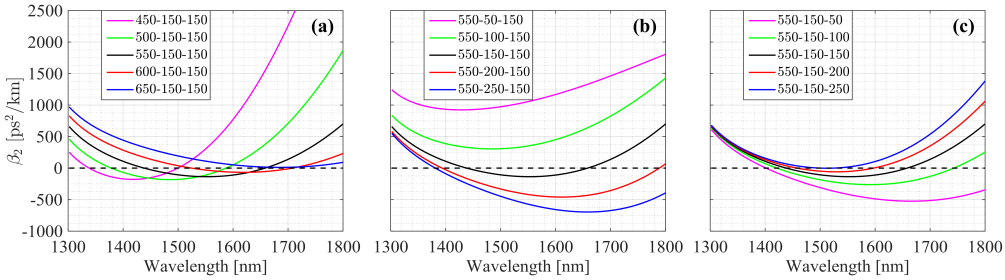

Fig. 2. (a). β_2 versus wavelength by setting W_c at 450 nm (magenta), 500 nm (green), 550 nm (black), 600 nm (red) and 650 nm (blue) for the dimensions of W_c-150-150. (b). β_2 versus wavelength by setting S at 50 nm (magenta), 100 nm (green), 150 nm (black), 200 nm (red) and 250 nm (blue) for the dimensions of 550-S-150. (c). β_2 versus wavelength by setting W_s at 50 nm (magenta), 100 nm (green), 150 nm (black), 200 nm (red) and 250 nm (blue) for the dimensions of 550-150-W_s.

Figure 2 shows the GVD parameter β_2 as a function of wavelength for different waveguide design. In Fig. 2(a), we consider how GVD depends on W_c, in the configuration W_c-150-150. Increasing the value of W_c results in a red shift of the zero-dispersion wavelengths. This tendency stops at W_c=650 nm, where β_2>0 for all considered wavelengths. Figure 2(b) shows the configuration 550-S-150, for which the GVD is normal when S=50 nm and S=100 nm, but exhibits an increasingly large wavelength region of anomalous GVD as S increases from 150 nm to 250 nm. Figure 2(c) shows the configuration 550-150-W_s, which results in anomalous GVD at telecom wavelengths for $S \leq 200$ nm. Noteworthy, the impact on GVD induced by varying W_s is much smaller than that induced by varying S.

As shown in Fig. 2, some waveguide dimensions result in two zero-dispersion wavelengths around 1550 nm. Such behavior is interesting from the perspective of achieving a spectrally-flattened near-zero GVD. In the following, we denote these two wavelengths as ZDW_S (short wavelength) and ZDW_L (long wavelength), respectively, and consider the case that the region in between is anomalous. We vary the three geometric parameters to make ZDW_S = 1460 nm and ZDW_L = 1625 nm, giving rise to anomalous GVD in a spectral region that covers S-, C- and L-band. More specifically, for a given W_c, we can find the suitable sets of S and W_s to make ZDW_S at 1460 nm and ZDW_L at 1625 nm, respectively. As shown in Fig. 3, the blue solid curve

Optics EXPRESS

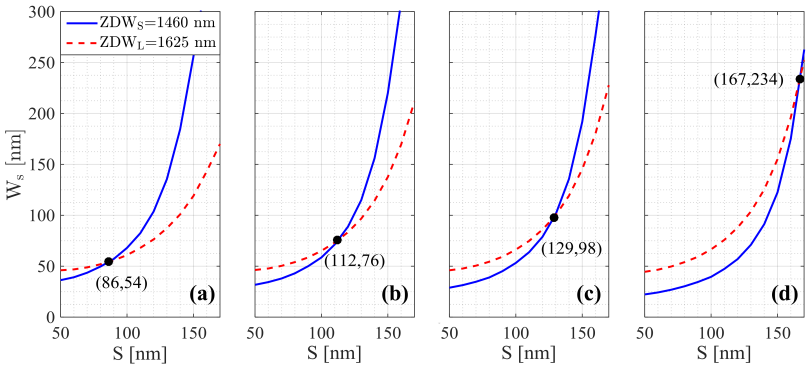

Fig. 3. The S-W$_s$ curve that makes ZDW$_S$ = 1460 nm (blue solid) and ZDW$_L$ = 1625 nm (red dashed), respectively. The core width and the related proposed dimension is: (a). W$_c$=520 nm and 520-86-54, (b). W$_c$=540 nm and 540-112-76, (c). W$_c$=550 nm and 550-129-98, (d). W$_c$=570 nm and 570-167-234.

represents the S-W$_s$ corresponding to ZDW$_S$ = 1460 nm, while the red dashed curve represents the S-W$_s$ corresponding to ZDW$_L$ = 1625 nm. Using the crossover point of the two curves, we get proposed dimensions of 520-86-54, 540-112-76, 550-129-98, and 570-167-234. Note that small W$_s$ helps to avoid the independent beam guidance of side-strip modes, while large S increases the silica filling ratio of the slots [31,32], which further mitigates the uncertainty of the actual GVD induced by partial filling. Therefore, there is a trade-off between W$_s$ and S, and we choose a suitable dimension of 550-129-98.

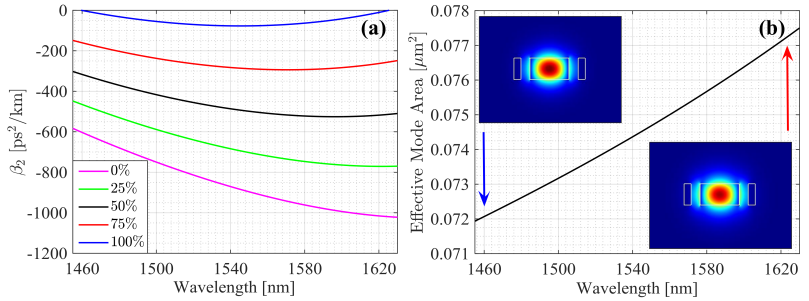

Fig. 4. (a). β_2 versus wavelength in the dimension of 550-129-98 by setting the average refractive index of slots at 1 (magenta), 1.11 (green), 1.22 (black), 1.34 (red) and 1.45 (blue). (b). Effective mode area A_{eff} versus wavelength. The insets are the mode profile at 1460 nm and 1625 nm, respectively.

We use the weighted average refractive index n_s, which has been widely used in photonic crystal fibers [35], to evaluate the filling ratio. Although such a simple calculation does not quantify the material distribution of the slots in detail, it remains valid to characterize the impact of partial filling of the slots. Figure 4(a) shows β_2 versus wavelength for the chosen dimension of 550-129-98, with n$_s$ varying from 1 (filling ratio of 0%), 1.11 (filling ratio of 25%), 1.22 (filling ratio of 50%), 1.34 (filling ratio of 75%) to 1.45 (filling ratio of 100%). At all wavelengths $|\beta_2|$ becomes larger with decreasing n$_s$. At 1550 nm, β_2 is -900 ps^2/km, -700 ps^2/km, -500 ps^2/km, -300 ps^2/km, when the filling ratio is 0%, 25%, 50%, 75%, respectively. Hence, the higher the filling ratio is, the smaller $|\beta_2|$ one gets. It is worth noting when the slots are 100% filled by silica, β_2 at all wavelengths is anomalous with a maximal value of $|\beta_2| = 60$ ps^2/km, which is one-tenth

Optics EXPRESS

of that for the corresponding strip structure without slots and side strips ($|\beta_2|$ = 600 ps^2/km).

Reducing the refractive index contrast of the slots and side strips facilitates near-zero GVD, but weakens the beam confinement in the center core. We simulate the effective mode area A_{eff} versus wavelength for the dimension of 550-129-98 with silica filling ratio of 100%. As shown in Fig. 4(b), A_{eff} increases from 0.072 μm^2 to 0.078 μm^2 with increasing wavelength. At 1550 nm, A_{eff} is 0.075 μm^2 for the proposed structure, which is larger than 0.066 μm^2 for the corresponding strip structure. Although the slots and the side strips result in 12% reduction of the nonlinear coefficient calculated by the ratio of the two effective mode areas, such reduction is often negligible in actual wavelength conversion applications. The insets in Fig. 4(b) are the intensity distributions at 1460 nm and 1625 nm, respectively. The field at 1460 nm is well confined in the core, while the beam at 1625 nm leaks more into the slots, which reveals that A_{eff} increases with increasing wavelength. Since dominant field is confined in the center core, the proposed dimension is expected to enable high-efficiency wavelength conversion.

3. Experimental measurement of wavelength conversion

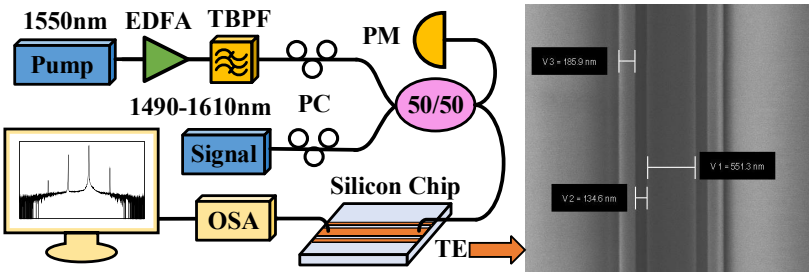

Fig. 5. A schematic experimental setup, and the Scanning Electron Microscope image from top view, where the dimension is measured at 551-135-186. The pump wavelength is 1550 nm with an in-waveguide power of 15 dBm. The signal is tuned within 1490 nm-1610 nm, with an in-waveguide power level of 0 dBm. Components abbreviation: EDFA: Erbium-doped fiber amplifier, TBPF: Tunable band-pass filter, PC: Polarization controller, PM: Power-meter, OSA: Optical spectrum analyzer.

Wavelength conversion experiment is often used to validate GVD tailoring. The conversion efficiency η, given by the ratio of the idler power to the signal power at output ($\eta = P_i/P_s$), is used to quantify the wavelength conversion. Although the nonlinear coefficient for the proposed structure is 88% of that for the corresponding strip structure, the bandwidth is predicted to be significantly broadened [7]. To verify this, we fabricated a waveguide sample by taking the following steps. First, a standard SOI nano-fabrication process, including e-beam lithography (JEOL-JBX-9500FS-EBL) and inductively coupled plasma (ICP) etching, was used to fabricate the fully etched photonic crystal based grating couplers (PCGCs) [36] and the silicon waveguide simultaneously. Then, the Scanning Electron Microscope (SEM) image from top view was taken to measure the actual dimension. We adjust W_s up to 190 nm, noting that it is not wide enough to guide independent mode inside, but makes $|\beta_2|$ smaller (see Fig. 3) so that the mode expansion induced by the partial filling in the slot can be suppressed (see Fig. 4). Due to fabrication uncertainty, the actual dimension was 551-135-186. Finally, a 1 μm-thick silica cladding was deposited by the plasma enhanced chemical vapor deposition.

A schematic experimental setup is shown in Fig. 5. A continuous-wave (CW) 1550 nm laser was used as the pump seed, and amplified by an erbium-doped fiber amplifier (EDFA), while the amplified spontaneous emission was filtered through a tunable band-pass filter (TBPF). A tunable CW laser was applied as the signal. Through a 50%-50% coupler, the pump and the

Optics EXPRESS

signal were combined, and the power was monitored by a powermeter (PM). Two polarization controllers (PCs) were used to optimize the polarization, so that a minimal alignment loss through the TE-polarized PCGCs was obtained. The propagation loss was measured to 3 dB/cm through a cut-back method, while the minimal insertion loss reached 15 dB. The transmittance of the PCGCs was symmetric at 1550 nm with a 3 dB bandwidth of 30 nm [36]. The output power of the signal and idler was measured through an optical spectrum analyzer (OSA).

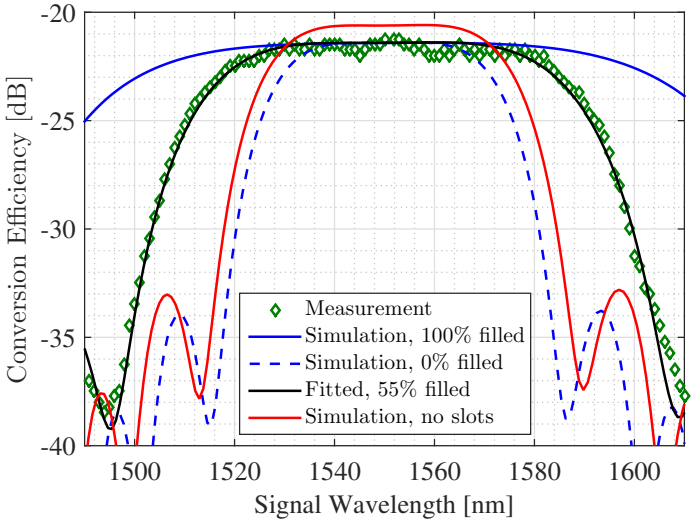

Fig. 6. Simulations and measurement of η in a wavelength range of 1490 – 1610 nm. Green diamond: measurement, blue solid: simulations when the filling ratio is 100%, blue dashed: simulations when the filling ratio is 0%, black solid: fitted simulations when the filling ratio is 55%, red solid: simulations of the corresponding strip structure.

We measured the conversion efficiency, η, versus signal wavelength (see Fig. 6 green diamond). We also simulated η versus signal wavelength based on the model in [37]. The in-waveguide power levels of the pump and the signal were set to 15 dBm and 0 dBm, respectively, in agreement with our experiments. The length of the waveguide was 1 cm, the linear loss was 3 dB/cm, the free carrier lifetime τ was 10 ns, other parameters were from [37]. Two extreme cases were considered during the simulation: the blue solid in Fig. 6 represents the case where the silica filling ratio was 100% resulting in a 3 dB bandwidth of 116 nm; the blue dashed in Fig. 6 represents the case where the silica filling ratio was 0% with a 3 dB bandwidth of 48 nm. This strongly highlights the importance of achieving a high filling ratio. As expected, however, the measurements resulted in a 3 dB bandwidth of 76 nm, which is in between the two extremes. Therefore, to estimate the filling ratio of our waveguide sample, we used it as a fitting parameter. The best fit (black solid) corresponds to a filling ratio of 55%. As a comparison, we also simulated η for the corresponding strip structure (red solid). The maximal η was 1 dB higher than the measurement, but the 3 dB bandwidth of 52 nm was smaller. Thus, even though the proposed structure has the same fabrication procedure as the strip structure, we achieved broadening of the 3 dB bandwidth by a factor of 1.5 using the vertical-dual-slot waveguide.

The experimental measurement proves that the proposed structure enables GVD tailoring, which is the first explicit proof of such a concept to our best knowledge. However, the proposed structure comes across a problem of fully filling the slots, which can, in future work, be addressed and solved by using other cladding deposition approaches, for example, atomic layer deposition, or employing angled sidewalls of both the center core and the side strips [31]. Moreover, other cladding materials can be considered to avoid the partial filling in the slots such as alumina and

Optics EXPRESS

titania produced through the atomic layer deposition [38]. Additionally, such a structure can be also applied to other on-chip platforms.

4. Conclusion

We have proposed a silicon waveguide structure that employs vertical-dual slots. Such a structure benefits from simple fabrication and flexibly tailorable group-velocity dispersion. We have accurately simulated the zero-dispersion wavelengths for the proposed structure, and obtained a spectrally-flattened near-zero anomalous group-velocity dispersion covering the whole telecom wavelength range. We have also fabricated the proposed waveguide sample, and demonstrated the wavelength conversion experiment achieving a measured 3 dB bandwidth of 76 nm, which is dramatically broadened compared to the corresponding strip waveguide, even with partial filling in the slots. Since the fabrication procedure of our proposed waveguide is the same as the standard strip waveguides, it has a potential to suffice various on-chip functionality using four-wave mixing.

Funding

This work is supported jointly by the Chinese Scholarship Council, the National Natural Science Foundation of China (Grant No. 61465015), and the center of excellence: Silicon Photonics for Optical Communications granted by the Danish National Research Foundation (DNRF123).